Supporting Information

Highly Active and Noble-Metal-Alternative Hydrogenation Catalysts Prepared by Dealloying Ni–Si Intermetallic compounds

Wiyanti F. Simanullang,[†] Hiroshi Itahara,[‡] Naoko Takahashi,[‡]

Satoru Kosaka,[‡] Ken-ichi Shimizu,[†,§] Shinya Furukawa,*[,†,§]

[†]*Institute for Catalysis, Hokkaido University, N-21, W-10, Sapporo 001-0021, Japan*

[‡]*Toyota Central Research & Development Labs., Inc., 41-1 Yokomichi Nagakute, Aichi 480-1192,*

Japan.

[§]*Elements Strategy Initiative for Catalysts and Batteries, Kyoto University, Katsura, Kyoto 615-8520,*

Japan

E-mail: furukawa@cat.hokudai.ac.jp,

Tel: +81-11-706-9162, Fax: +81-11-706-9163

Experimental details

Catalyst Preparation

Ni–Si materials and Ni_3Al (crushed powder) were supplied from Kojundo Chemical Lab. Co. Ltd (synthesized by arc melting: Ni_3Si, 98%, 45 μm; Ni_2Si, NiSi, and $NiSi_2$, 99.9%, 50 μm; Ni_3Al, 93%, 45 μm). Ni_3Sn and Ni_3Ge intermetallic compunds were prepared by arc melting using metal beads (Soekawa Chemical, 99.9% for each). The resultant ingots were crushed in air and filtered into particles with diameters below 25 μm. For catalytic use, Ni powder (Wako, 99%, 150 μm) and Pd black (Wako, 97%) were used. The intermetallic compound power (1.0 g) was added into a vigorously sttired aqueous solution of hydrofluoric acid (HF, 0.2~5.0 M, 15 ml) in a 100 ml teflon beaker and kept for 15 min at room temperature in the air. The treated material was collected by centrifugation and washed with deionized water three times, followed by drying at 80°C.

Ni nanoparticles supported on silica gel were prepared by pore-filling impregnation method. Aqueous solution of $Ni(NO_3)_3 \cdot 6H_2O$ (Wako, 99%) was added to dried silica gel (CARiACT G-6, Fuji Silysia, $S_{BET} = 470$ m^2 g^{-1}) so that the solutions filled the silica pores. The mixtures were sealed overnight at room temperature and dried over a hot plate, followed by reduction under flowing H_2 at 600 °C for 1 h.

Reaction condition

Catalytic performances of the prepared catalysts were tested in hydrogenation of ethylene, acetylene, toluene, and benzene. The mixture of the Ni-based catalyst (typically, 30 mg, treated with 1.0 M HF) and quartz sand (Miyazaki Chemical Co., 250 ~ 420 μm, 2 g) was filled into a quartz glass tube (internal diameter, 10 mm) and put in a fixed bed continuous flow reactor. Prior to the activity test, the catalyst was reduced under flowing H_2 (10 ml/mim) at 400°C for 0.5 h. The reaction was initiated by flowing the reaction mixture: (a) ethylene to ethane (C_2H_4 : H_2 : He = 10 : 10 : 30 ml/min, 70°C), (b) acetylene to ethylene and ethane (C_2H_2 : H_2 : He = 2 : 10 : 30 ml/min, 150°C), (c) toluene to methylcyclohexane (C_7H_8 : H_2 : He = 0.2 : 5 : 10 ml/min, 150°C) and (d) benzene to cyclohexane (C_6H_6 : H_2 : He = 0.7 : 5 : 10 ml/min, 150°C). The gas phase was analyzed by an online thermal conductivity detector (TCD) gas chromatography (Shimadzu GC-8A) equipped downstream. Turnover frequency (TOF/ s^{-1} or min^{-1}) was calculated as the product formation rate (mmol/s^{-1} or min^{-1}) per the number of active Ni sites (mmol), which was determined by CO pulse chemisorption noted below.

Characterization

The crystal structure of the prepared catalyst was examined by powder X-ray diffraction (XRD) by a Rigaku MiniFlex II/AP diffractometer with Cu   Kα radiation.

X-Ray Photoelectron Spectroscopy (XPS) analysis was conducted using ULVAC PHI Quantera SXM with monochromatic Al Kα X-rays at 1486.6 eV, 14 kV and 1500 W. Spectra were measured for the sample after heat treatment under a 5% H_2/Ar flow (500 mL min^{-1}) at 673 K for 0.5 h. The base pressure was set below 1.0×10^{-7} Pa. The diameter of detection and the take-off angle (TOA) were 400 μmΦ and 45°, respectively. Here, the surface normal corresponds to a TOA of 90°. The pass energy and the energy step were set at 29.35 eV and 0.125 eV, respectively. The binding energies were calibrated based on the hydrocarbon C1s peak at 285 eV.

The angular-resolved Hard X-ray Photoelectron Spectroscopy (HAXPES) measurements were conducted on the SPring-8 BL16XU beamline as described in the previous report.[1] The photon energy was set at 7946.6 eV for Ni2p$_{3/2}$ and Si 2p core levels. The energies and angular distributions of the photoelectrons were assessed using a VG-Scienta R4000-HV hemispherical analyzer. The objective lens has an effective acceptance angle of approximately ±30° and an angular resolution of 1.32°. The stability of the system was confirmed using the Au 4f$_{7/2}$ photoelectron peak for an Au film on a Si substrate. The overall stability of the photoelectron energy was found to be within 50 meV. The angular distributions of the photoelectrons were determined at photoelectron take-off angles at 85°. Here, a take-off angle perpendicular to the surface is defined as 90°. The analysis depths of the HAXPES measurements were calculated according to the previous report.[2]

The X-ray adsorption fine structure (XAFS) spectra of Ni K-edge were recorded by fluorescence mode at SPring-8 BL16B2. The angle between the sample surface and the direction vector of incident X-rays was 45°, and the spectra were acquired by solid state detector. The X-ray irradiated area on the sample surface was 1 mm (vertical) x 2 mm (horizontal). The Near edge X-ray adsorption fine structure (NEXAFS) spectra of Si K-edge were recorded by fluorescence mode at Aichi SR BL6N1. The angle between the sample surface and the direction vector of incident X-rays was 90°, and the spectra were acquired by silicon drift detector. The X-ray irradiated area on the sample surface was 1 mm (vertical) x 2 mm (horizontal).

The microstructure of the samples was observed by scanning electron microscopy (SEM; Hitachi High-Technologies S-5500), transmission electron microscopy (TEM; JEOL JEM-2100F), and scanning transmission electron microscopy with energy dispersive X-ray analysis (STEM-EDX; FEI Talos F200X, at 200 kV). For STEM observation, a cross-section of the sample was prepared using focused ion beam (FIB: FEI, Helios, thickness: 100 nm).

CO pulse chemisorption was performed using BELCAT II (Microtrac BEL) to estimate the Ni and Pd dispersion of the prepared catalysts. Prior to chemisorption, the catalyst was pretreated under a 5% H_2/Ar flow (40 mL min^{-1}) at 400°C for 0.5 h. Because of the low metal dispersion of bulk materials, the catalyst amount was typically 100~300 mg to quantify sufficient amount of CO chemisorbed. After the reduction pretreatment,

He was introduced at the same temperature for 10 min to remove the chemisorbed hydrogen, followed by cooling to room temperature. A 10% CO/He pulse was introduced into the reactor, and the supplied CO flow was quantified downstream by a TCD. For each sample, the CO chemisorption was performed at least three times (error was below 5%) and the averaged value was reported.

Computational details

Periodic DFT calculations were performed using the CASTEP code[3] with Vanderbilt-type ultrasoft pseudopotentials[4] and the revised version of the Perdew−Burke−Ernzerhof exchange−correlation functional based on the generalized gradient approximation.[5] The plane-wave basis set was truncated at a kinetic energy of 350 eV and a Fermi smearing of 0.1 eV was utilized. Dispersion correlations were considered using the Tkatchenko–Scheffler method with a scaling coefficient of $s_R = 0.94$ and a damping parameter of $d = 20$.[6] The reciprocal space was sampled using a k-point mesh with a spacing of typically 0.04 Å^{-1}, as generated by the Monkhorst−Pack scheme.[7] Geometry optimization was performed on supercell structures using periodic boundary conditions. The flat surface was modeled based on Ni(111)-(3 × 3) or Ni$_3$Si-(2 × 2) slab that was four atomic layers thick with 13 Å of vacuum spacing. To model a SiO$_2$ matrix within a limited computational resource, we adopted a β-tridymite structure (space group: $P6_3$/mmc, a high-temperature polymorph of quartz) as a crystalline SiO$_2$ with high symmetry. The supercell was model based on a (3 × 3 × 2) structure of β-tridymite with surface termination by O–H at each axial O–Si moiety and with 13 Å of vacuum spacing. A cavity was made by removing four SiO$_4$ units at the surface and with surface termination by O–H. For the model of Ni cluster, Ni$_{20}$ with a truncated octahedron structure was chosen so that the cluster just fitted within the cavity. The convergence criteria for structure optimization and energy calculation were set to (a) an SCF tolerance of 1.0×10^{-6} eV per atom, (b) an energy tolerance of 1.0×10^{-5} eV per atom, (c) a maximum force tolerance of 0.05 eV Å^{-1}, and (d) a maximum displacement tolerance of 1.0×10^{-3} Å. The transition state search was performed using the complete linear synchronous transit/quadratic synchronous transit (LST/QST) method.[8, 9] Linear synchronous transit maximization was performed, followed by energy minimization in the directions conjugating to the reaction pathway. The approximated TS was used to perform QST maximization with conjugate gradient minimization refinements. This cycle was repeated until a stationary point was found. Convergence criteria for the TS calculations were set to root-mean-square forces on an atom tolerance of 0.10 eV Å^{-1}.

Table S1. Catalytic performances of various Ni-based catalysts in ethylene hydrogenation. [a]

entry	catalyst	S_{BET} [b] / m^2g^{-1}	amount / mg	conv. (%)	TOF / s^{-1}	relative activity [c]	
						rate	TOF
1	Ni	0.50	300	37	2.1	1.0	1.0
2	Ni-HF	1.40	300	15	1.2	0.4	0.6
3	Ni/SiO$_2$		30	8	3.7	2.2	1.8
4	Ni$_3$Si		30	0.0	0.0	0.0	0.0
5	Ni$_3$Si-HF	0.94	30	29.0	41.1	7.8	19.9
6	Ni$_2$Si-HF		30	1.0	1.8	0.3	0.9
7	NiSi-HF		30	5.0	9.4	1.4	4.5
8	NiSi$_2$	0.49	30	0.0	0.0	0.0	0.0
9	NiSi$_2$-HF	0.79	10	25.0	15.4	20.3	7.4
10	Ni$_3$Al-HF	0.87	30	14.0	6.2	3.8	3.0
11	Ni$_3$Ge-HF		30	0.0	0.0	0.0	0.0
12	Ni$_3$Sn-HF		30	0.0	0.0	0.0	0.0

[a] Reaction condition: catalyst 10, 30, or 300 mg, quartz sand 2 g, C_2H_4:H_2:He = 10:10:30 ml min^{-1}, temp 70°C. [b] Specific surface area determined by N_2 adsorption method based on Brunauer–Emmett–Teller theory. [c] Relative value compared with Ni. [c] Relative value compared with Ni.

Table S2. Catalytic performances of Ni, Ni$_3$Si-HF, and NiSi$_2$-HF in hydrogenation of various unsaturated hydrocarbons.

reactant	temp. / °C	catalyst	amount / mg	conv. (%)	TOF	relative activity	
						rate	TOF
ethylene					(s^{-1})		
	70	Ni	300	37	2.1	1.0	1.0
	70	Ni$_3$Si-HF	30	29	41.1	7.8	19.9
	70	NiSi$_2$-HF	10	25	15.4	20.3	7.4
acetylene					(s^{-1})		
	150	Ni	100	1	0.2	1.0	1.0
	150	Ni$_3$Si-HF	100	8	3.4	8.0	20.3
	150	NiSi$_2$-HF	100	24	1.5	24.0	8.8
toluene					(min^{-1})		
	150	Ni	300	6	0.5	1.0	1.0
	150	Ni$_3$Si-HF	100	4	2.3	2.0	5.1
	150	NiSi$_2$-HF	30	12	3.4	20.0	7.3
benzene					(min^{-1})		
	150	Ni	200	8	2.0	1.0	1.0
	150	Ni$_3$Si-HF	100	13	24.9	3.3	12.4
☐	150	NiSi$_2$-HF	100	55	15.2	13.8	7.6

[a] Gas composition: C_2H_4:H_2:He = 10:10:30 ml min^{-1}, C_2H_2:H_2:He = 2:10:30 ml min^{-1}, C_7H_8:H_2:He = 0.2:5:10 ml min^{-1}, C_6H_6:H_2:He = 0.7:5:10 ml min^{-1}. [b] Relative value compared with Ni.

Table S3. Summary of catalytic performances of NiSi$_2$-HF, Pd, and Ni catalysts in hydrogenation of benzene and toluene.

catalyst	amount (mg)	dispersion (%)	Conv. at 8 h (%)		TOF at 8 h (min^{-1})		TON at 8 h	
			benzene	toluene	benzene	toluene	benzene	toluene
NiSi$_2$-HF	200 (102)[a]	0.128	89	93	10.4	3.8	5185	1786
Pd	100	0.179	46	96	6.9	5.3	3038	2513
Ni	200	0.024	3	5	0.3	0.3	205	166

[a] Ni content included in the whole catalyst.

Table S4. List of Hirshfeld charges on Ni atoms calculated by DFT.

atom No.[a]	Ni$_{20}$	Ni@SiO$_2$	Δ	atom No.[a]	Ni$_{20}$	Ni@SiO$_2$	Δ
1	0.02	0.02	0	11	0	0.02	0.02
2	0	0.02	0.02	12	-0.02	-0.01	0.01
3	0.02	0.02	0	13	-0.01	0.02	0.03
4	-0.03	-0.05	-0.02	14	-0.03	-0.05	-0.02
5	0.02	-0.02	-0.04	15	-0.01	-0.03	-0.02
6	0.01	-0.04	-0.05	16	-0.01	-0.03	-0.02
7	-0.03	0.03	0.06	17	-0.02	-0.03	-0.01
8	0	-0.05	-0.05	18	-0.02	-0.03	-0.01
9	-0.02	-0.01	0.01	19	0	0	0
10	-0.01	-0.05	-0.04	20	-0.01	0	0.01

The numbering of Ni atoms are indicated in Figure S8d. In most cases, difference in atomic charge was less than 0.03. Particularly for No. 3 Ni atom, which corresponds to that absorbs ethylene, no difference in atomic charge was observed. These demonstes that the effect of SiO$_2$ matrix on the atomic charge of Ni is negligible.
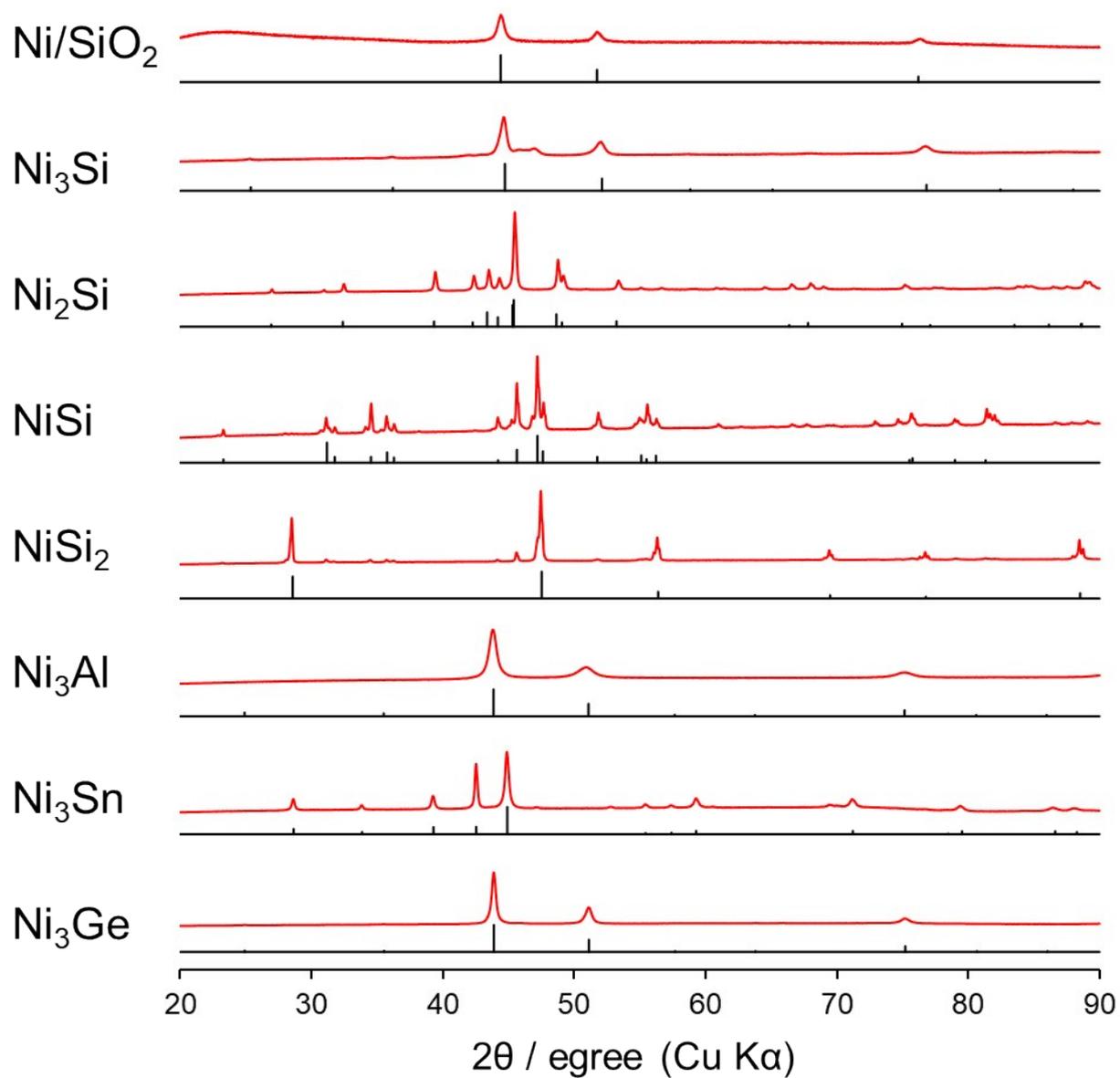
Figure S1. XRD patterns of Ni/SiO$_2$ and Ni-based intermetallic compounds. References are shown as black vertical lines. The desired intermetallic phases were observed with high phase purities.
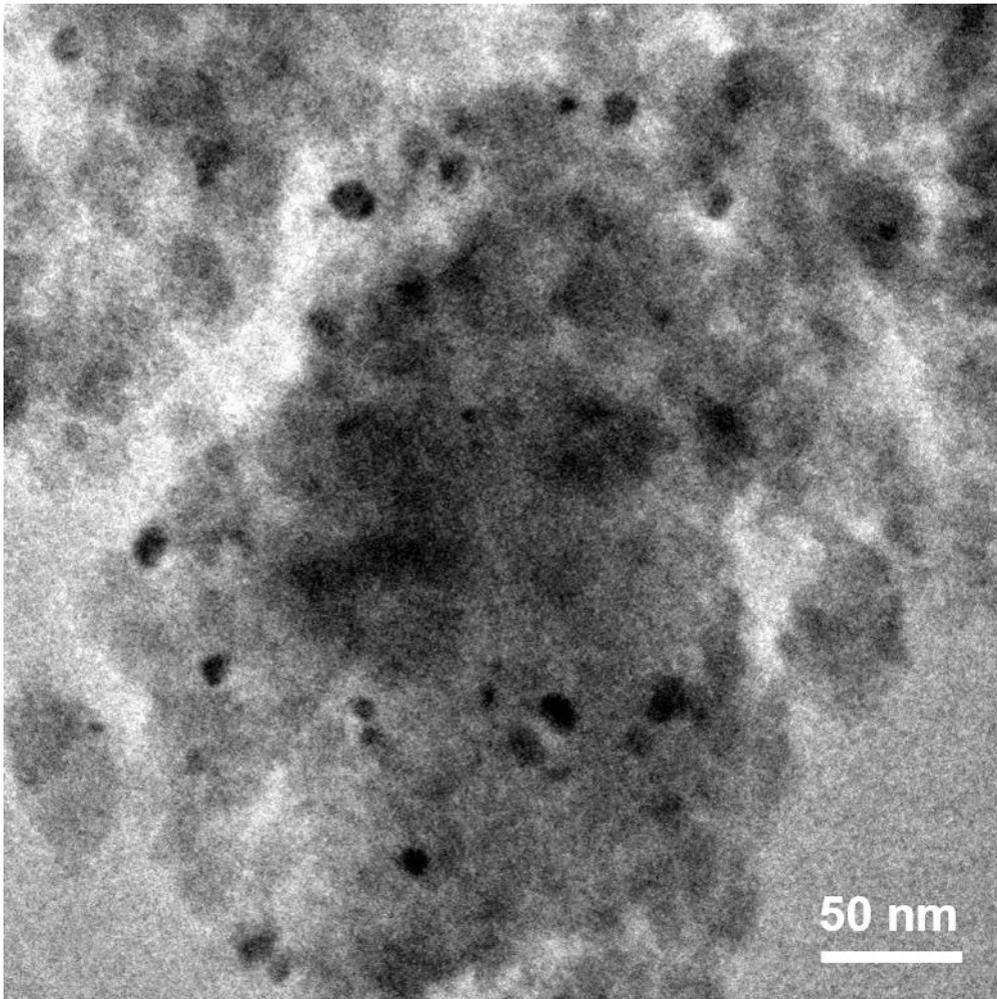
Figure S2. TEM image of Ni/SiO$_2$. Ni nanoparticles with the size of 7~10 nm are observed.
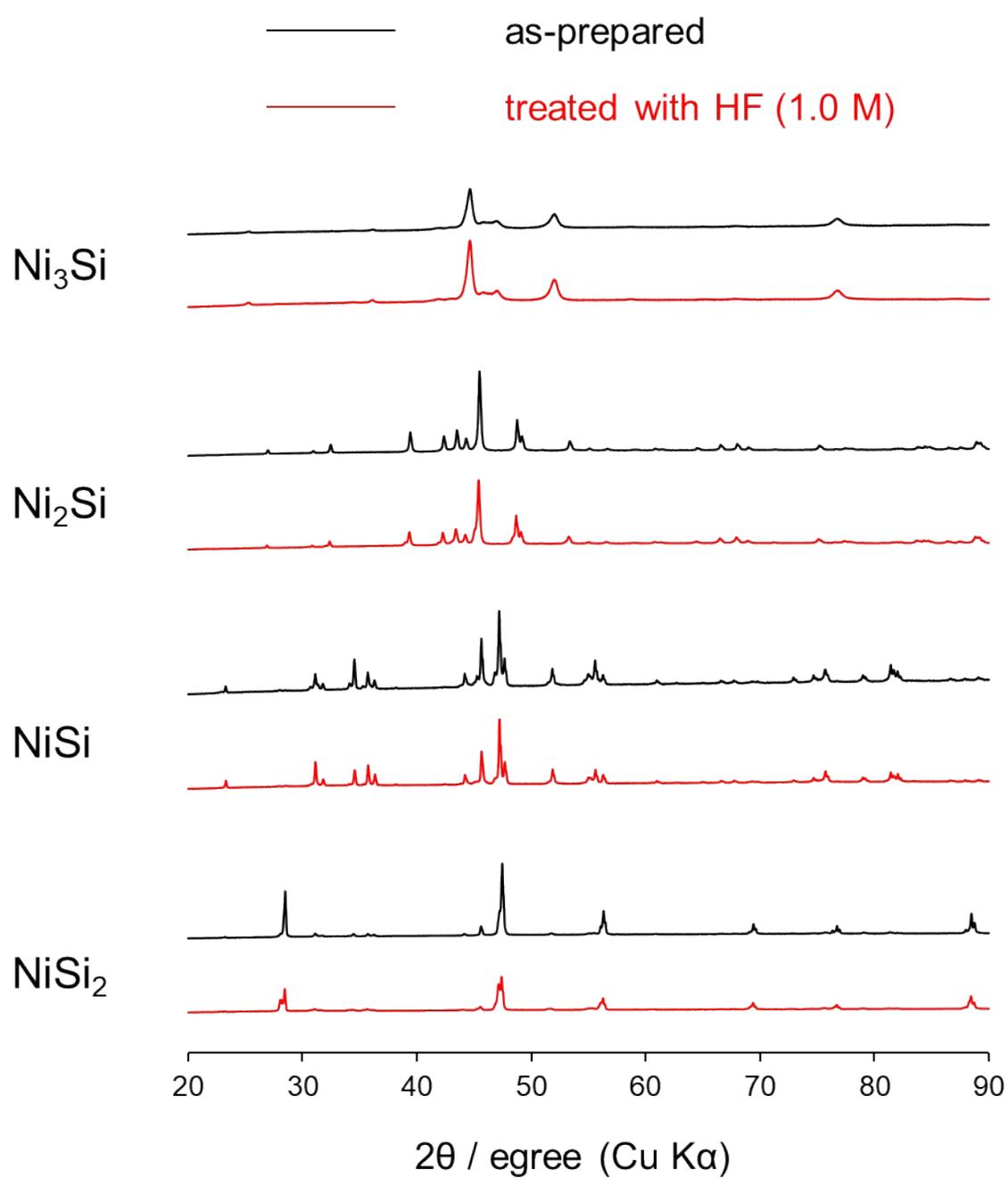
Figure S3. XRD patterns of Ni–Si intermetallic compounds before and after HF treatment. The parent intermetallic phases remained even after HF treatment, indicating that the bulk structure of each intermetallic compound was retained.
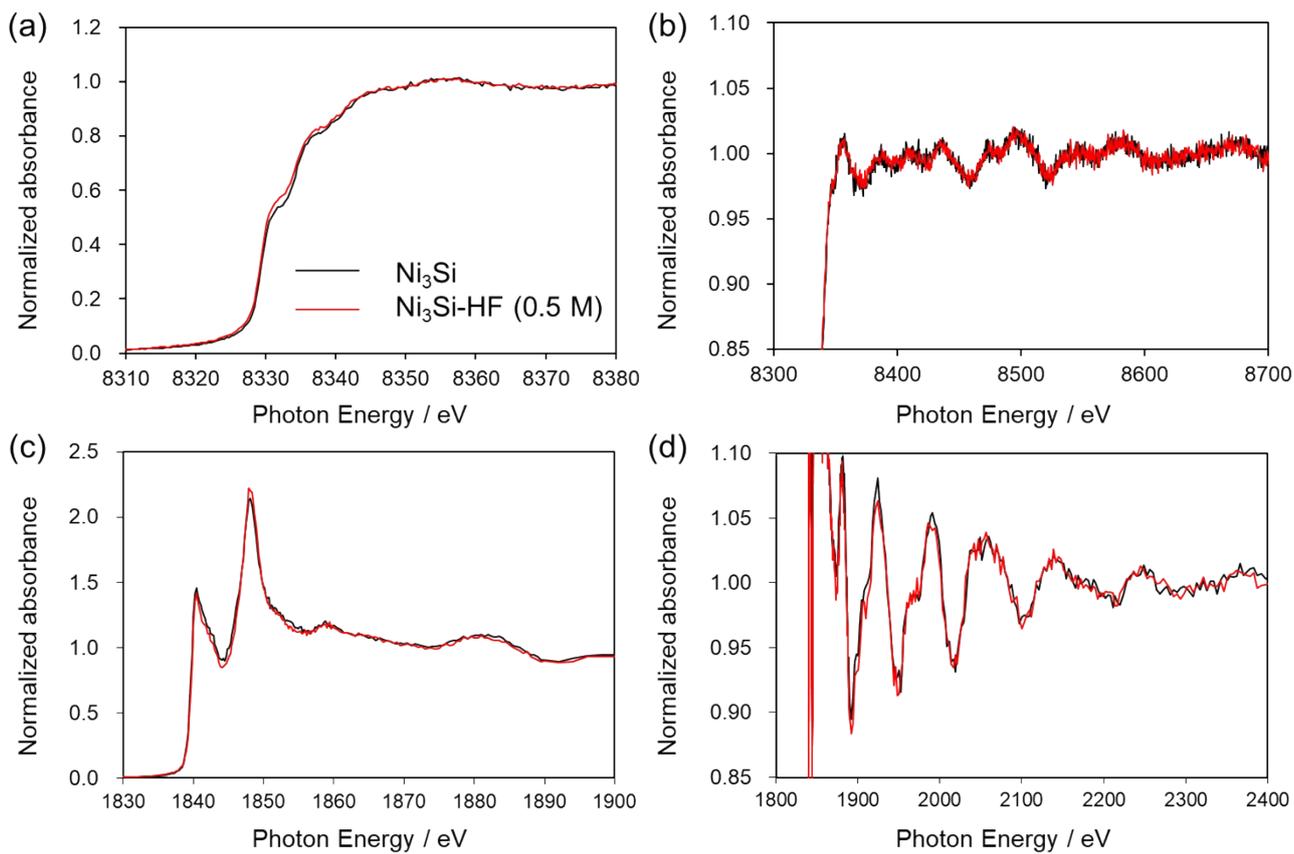
Figure S4. Normalized XAFS spectra of Ni_3Si with and without HF treatment (0.5 M): Ni K-edge (a) XANES and (b) EXAFS regions and Si K-edge (c) XANES and (d) EXAFS regions. No obvious change was observed after HF treatment, indicating that bulk structure of Ni_3Si was retained.
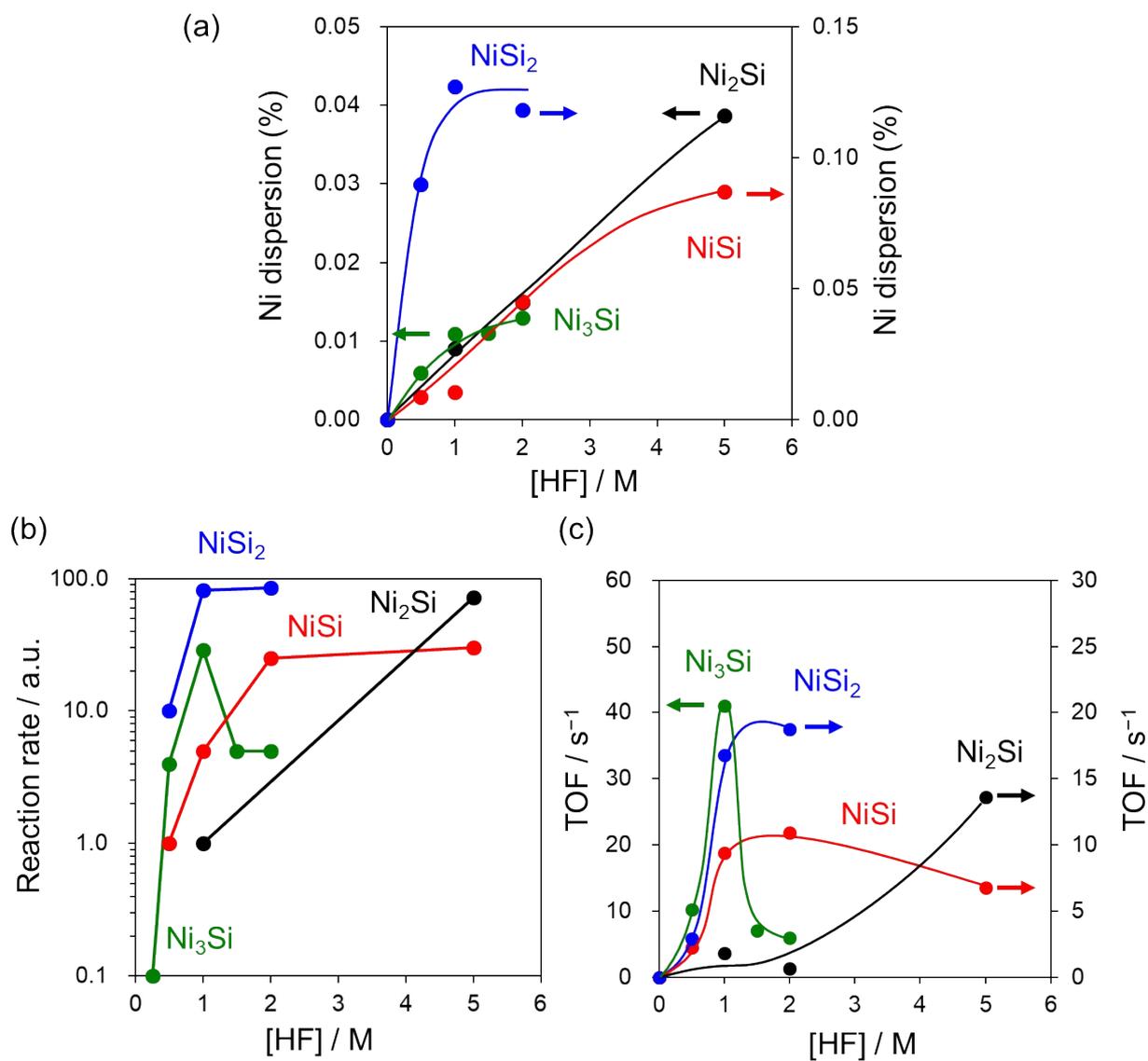
Figure S5. Effect of HF concentration on various properties of Ni–Si-HF catalysts: (a) Ni dispersion, (b) reaction rate, and (c) TOF in ethylene hydrogenation.

NiSi$_2$ NiSi$_2$-HF

(a)   (b)

2.0kV x500 SE   100um   2.0kV x500 SE   100um

(c)   (d)

2.0kV x5.00k SE   10.0um   2.0kV x5.00k SE   10.0um

(e)   (f)

2.0kV x20.0k SE   2.00um   2.0kV x20.0k SE   2.00um
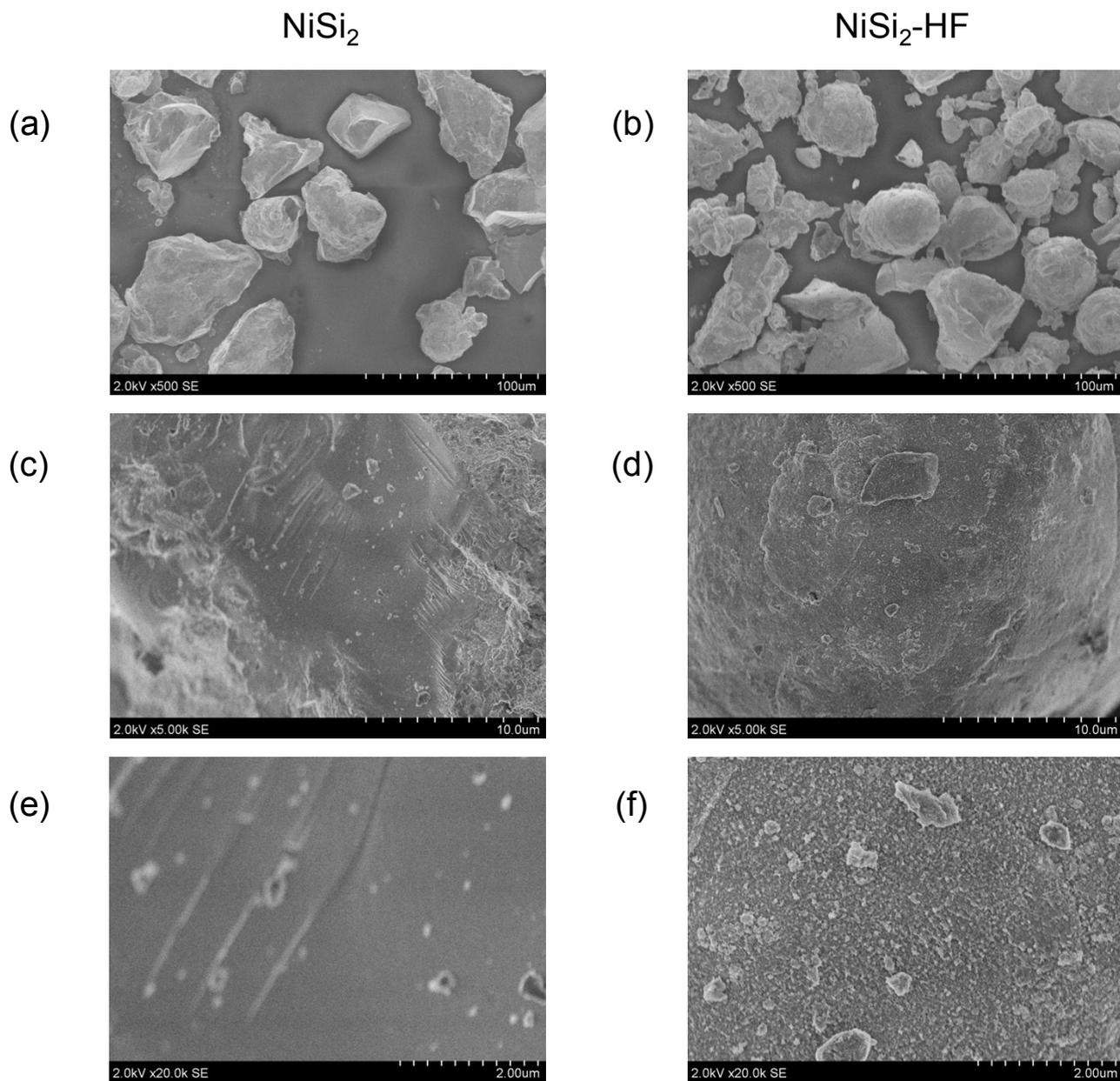
Figure S6. SEM images of NiSi$_2$ before (a, c, and e) and after (b, d, and f) HF (1.0 M) treatment. (a) and (b): wide range (×500) images for size distribution, (c) and (d): surface images (×5,000) of single particles, (e) and (f): close up (×20,000) of (c) and (d), respectively. Particles sizes are approximately 50 μm for the samples before and after HF treatment.
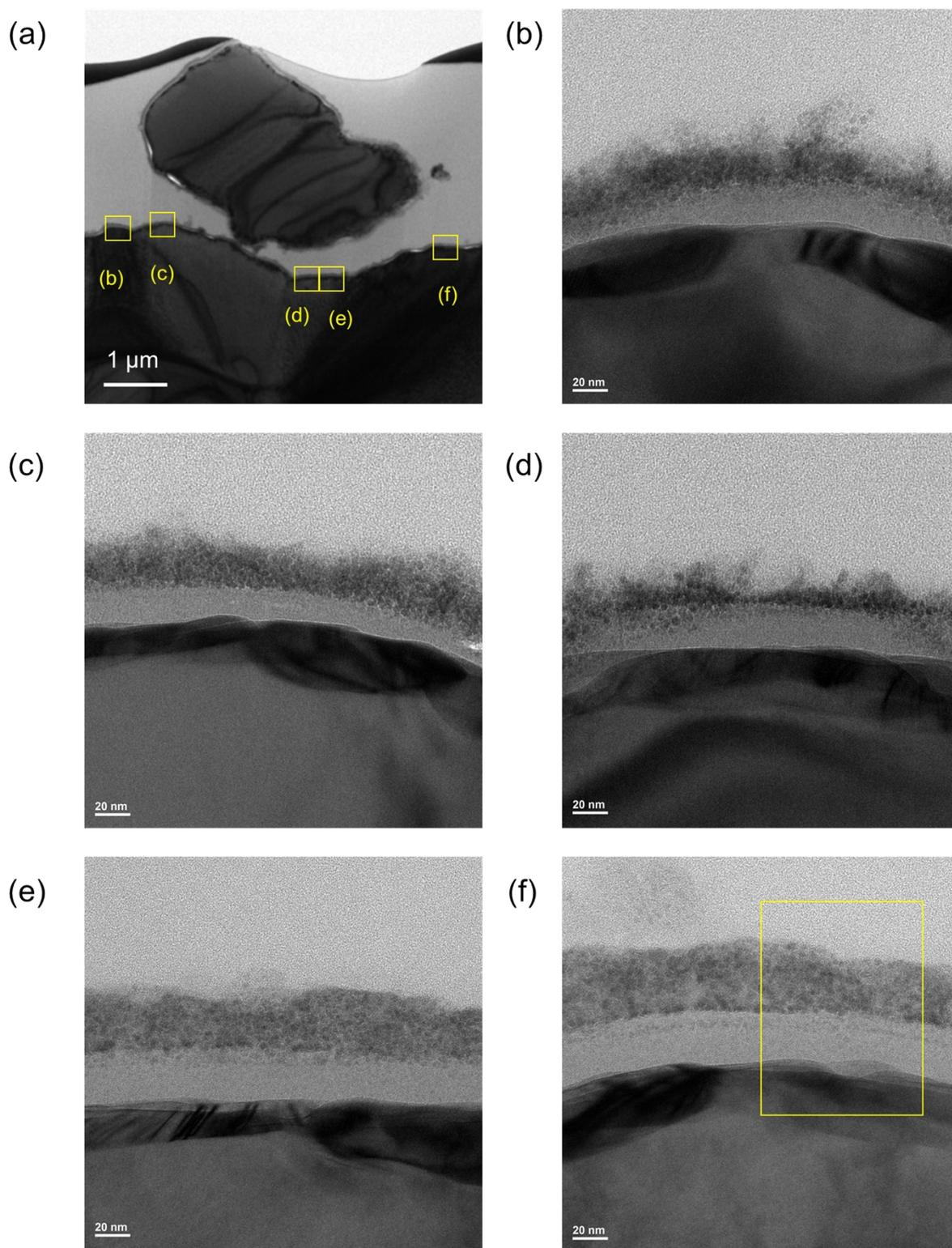
Figure S7. Bright-field STEM images of NiSi$_2$-HF (1.0 M) in cross-section: (a) wide range and (b)~(f) magnification. The large yellow square in (f) corresponds to the region shown in Figure 4d.
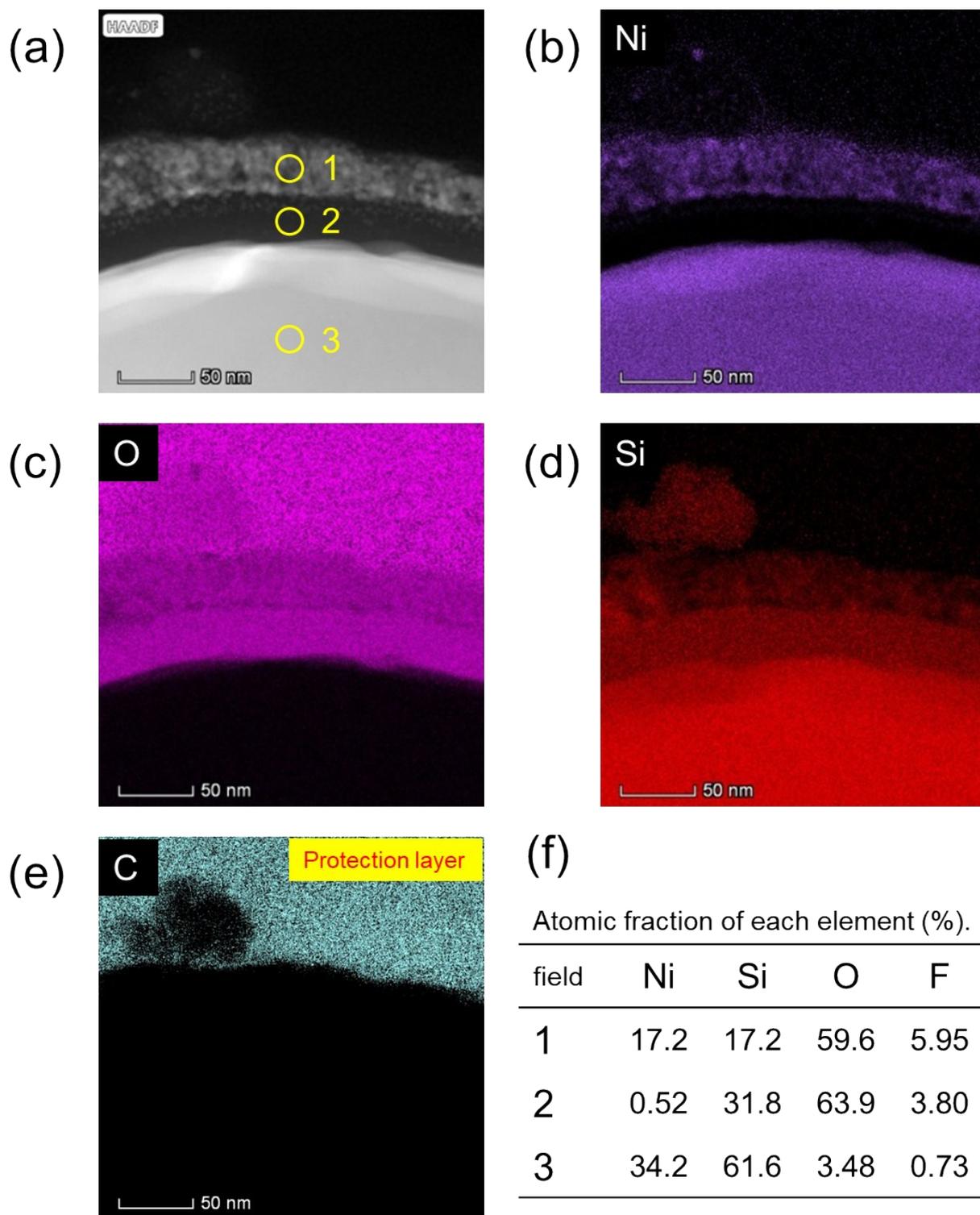
Figure S8. (a) High angle annuler dark-filed STEM image of the region shown in Figure S6f, elemental maps of (b) Ni, (c) O, (d) Si, and (e) C, and (f) atomic fraction of Ni, Si, O, and F. The organic protection layer used for the sample preparation by FIB is observed as C and O. The atomic fraction at each filed indicates the that each layer is consisted of (1) $NiO+SiO_2$, (2) SiO_2, and (3) $NiSi_2$. Only a small amount of F species remains at the surface region. The surface Ni species has been oxidized because of aerobic oxidation. The edge of $NiSi_2$ phase becomes Ni-rich than the bulk region, probably due to Si leaching during the HF treatment.

Atomic fraction of each element (%).

field	Ni	Si	O	F
1	17.2	17.2	59.6	5.95
2	0.52	31.8	63.9	3.80
3	34.2	61.6	3.48	0.73
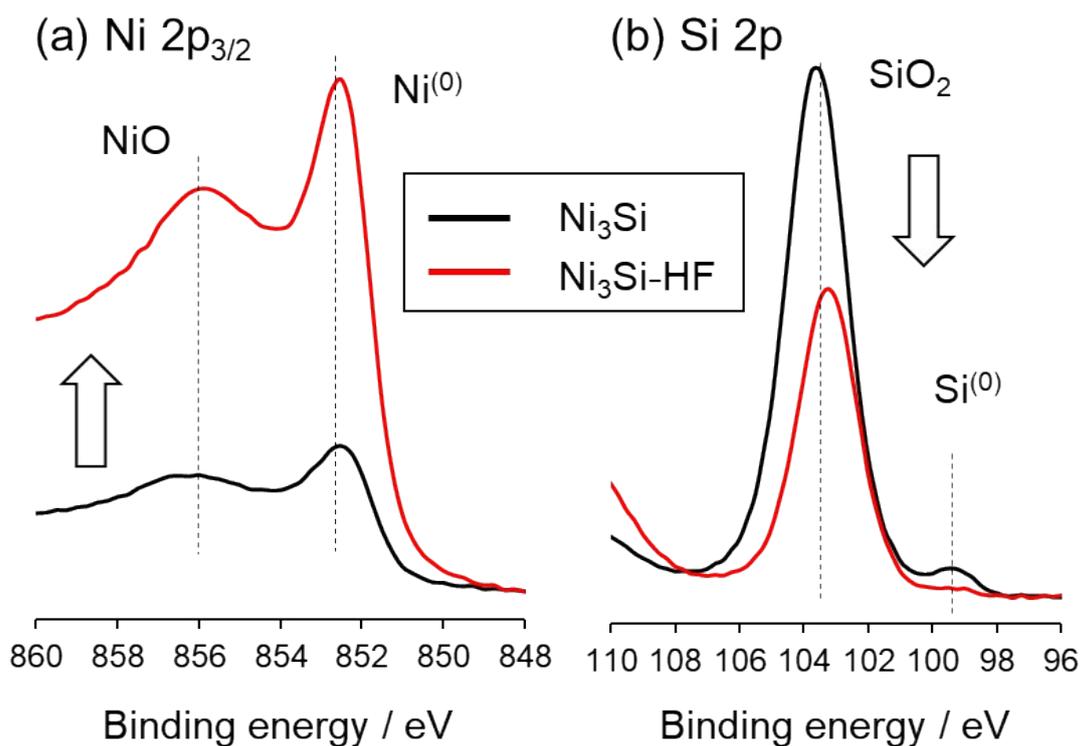
Figure S9. (a) Ni $2p_{3/2}$ and (b) Si 2p XPS of Ni$_3$Si before and after HF treatment. There is few Si(0) species for untreated Ni$_3$Si, indicating that the surface is covered with SiO$_2$.
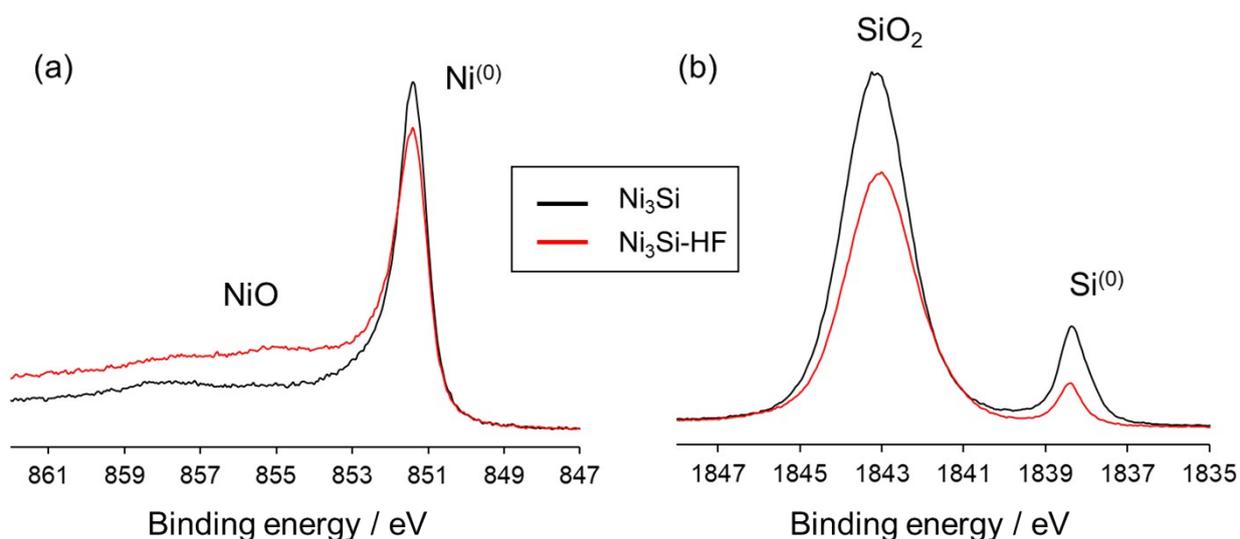
Figure S10. Hard X-ray photoelectron spectra of Ni$_3$Si before and after HF treatment (0.5 M): (a) Ni $2p_{3/2}$ and (b) Si 1s regions. Untreated Ni$_3$Si showed an intense peak assignable to SiO$_2$, indicating that SiO$_2$ was the main species even at the near surface region (>20 nm).
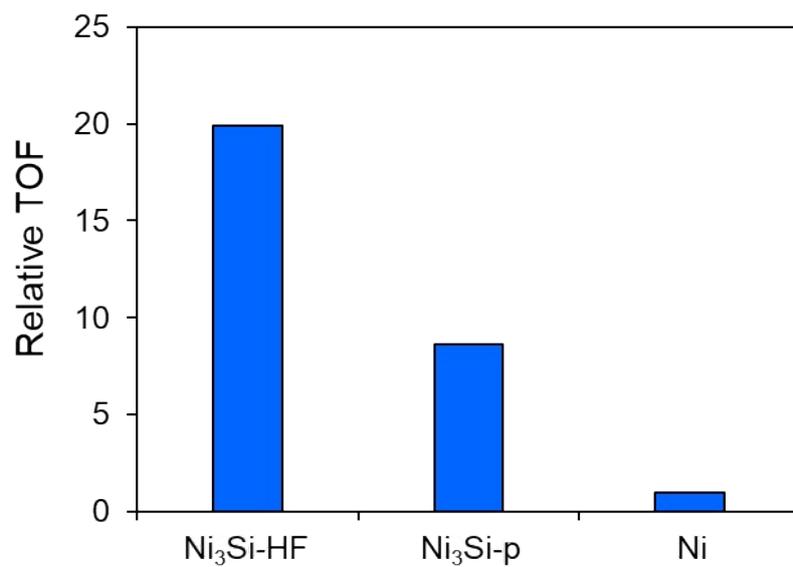
Figure S11. Relative TOF of Ni$_3$Si-HF, Ni$_3$Si-p, and Ni in ethylene hydrogenation at 70 °C.
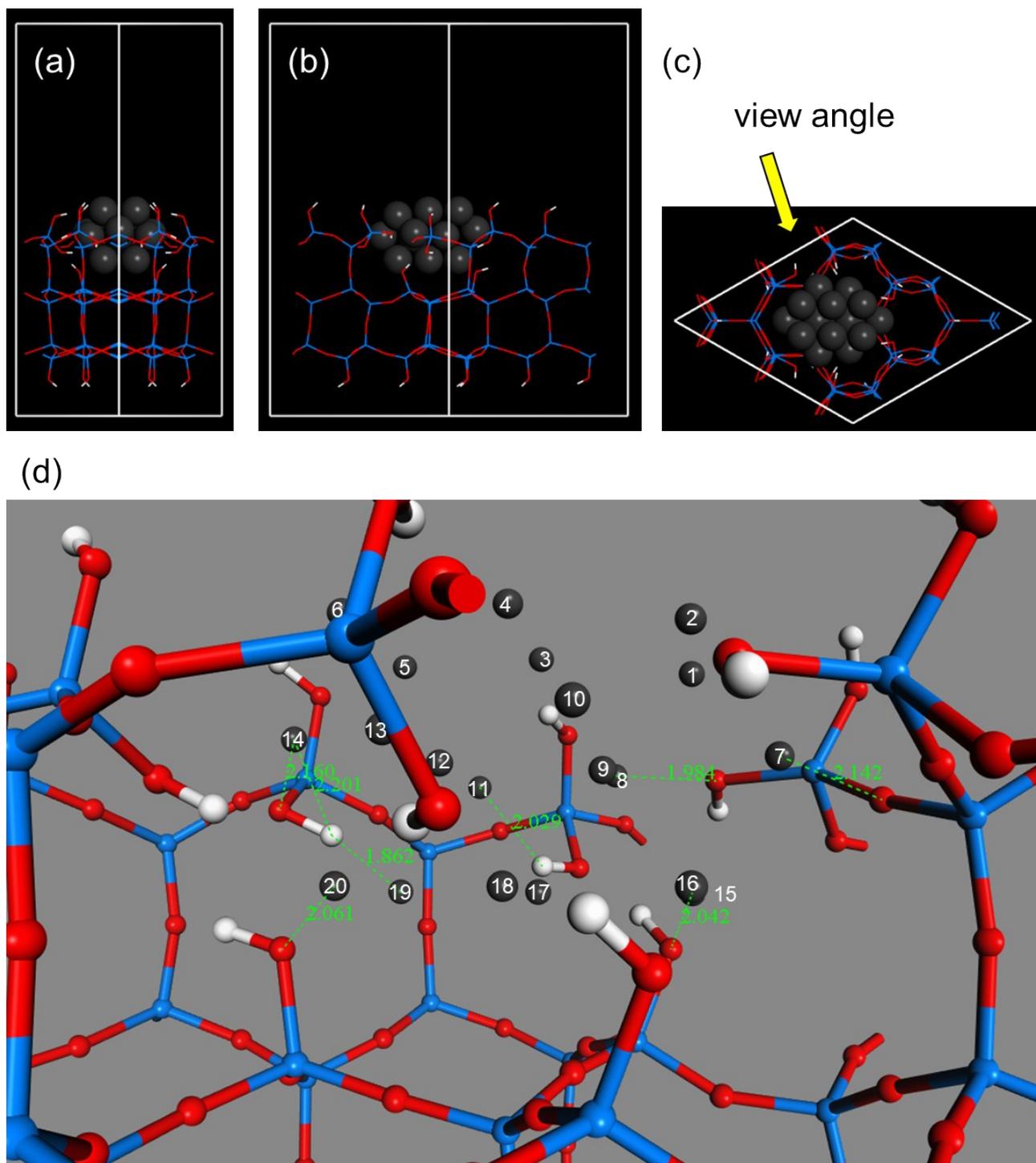
Figure S12. Optimized structure of Ni$_{20}$ cluster embedded in SiO$_2$ matrix viewed along (a) x, (b) y, and (c) z axes. Dark grey: Pd, blue: Si, red: O, white: H. (d) Representative close contact between Pd and lattice oxygen or OH group of SiO$_2$. Distances below 2.5 Å are shown. View angle is designated in the yellow arrow in (c). White labels indicate the numbering of Ni atoms.
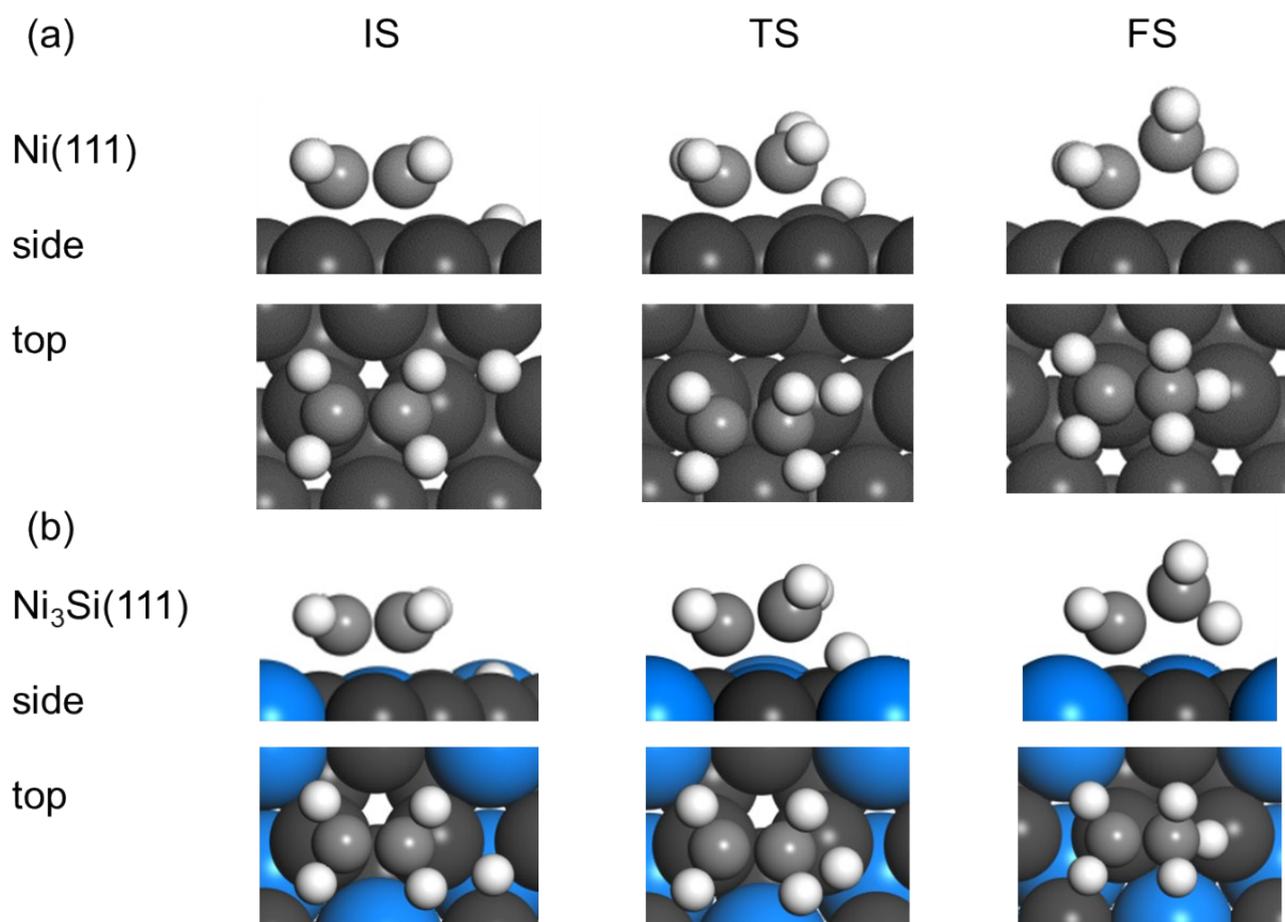
Figure S13. Structures of initial (IS), transition (TS), and final states (FS) for hydrogen attacke to ethylene adsorbed on (a) Ni(111), (b) Ni3Si(111), (c) Ni_{20} cluster, and (d) Ni_{20} embedded in SiO_2 matrix: (c) and (d) are shown in the following pages.
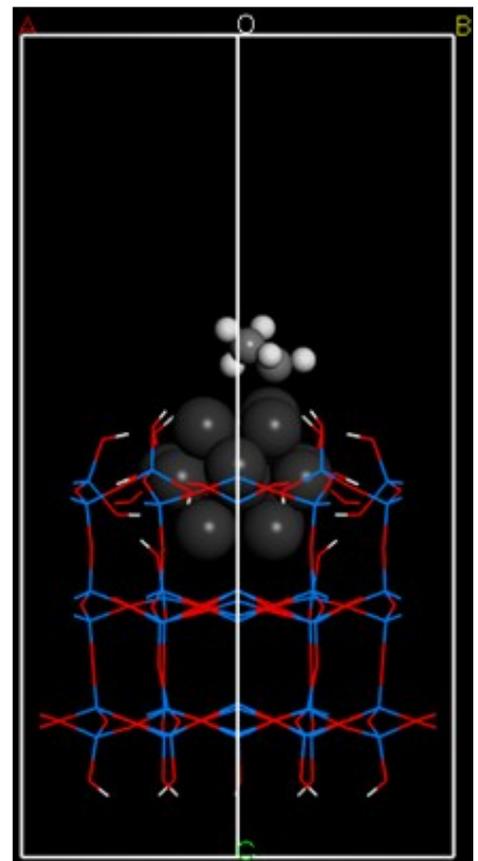
(c)   IS
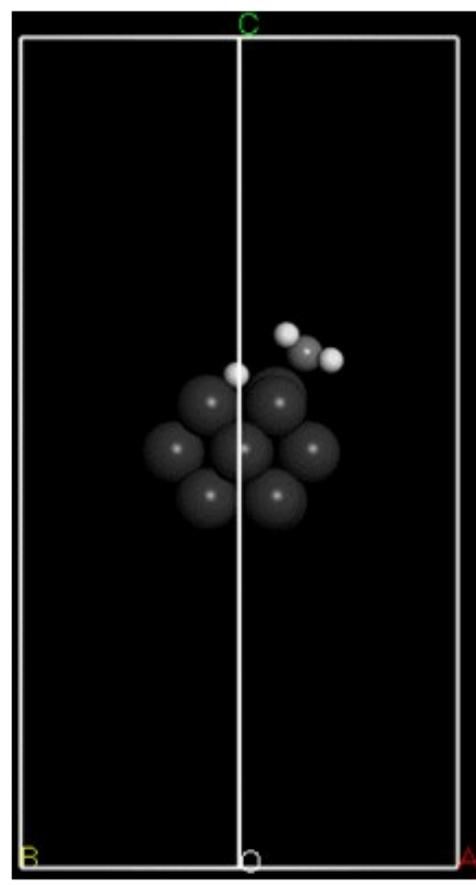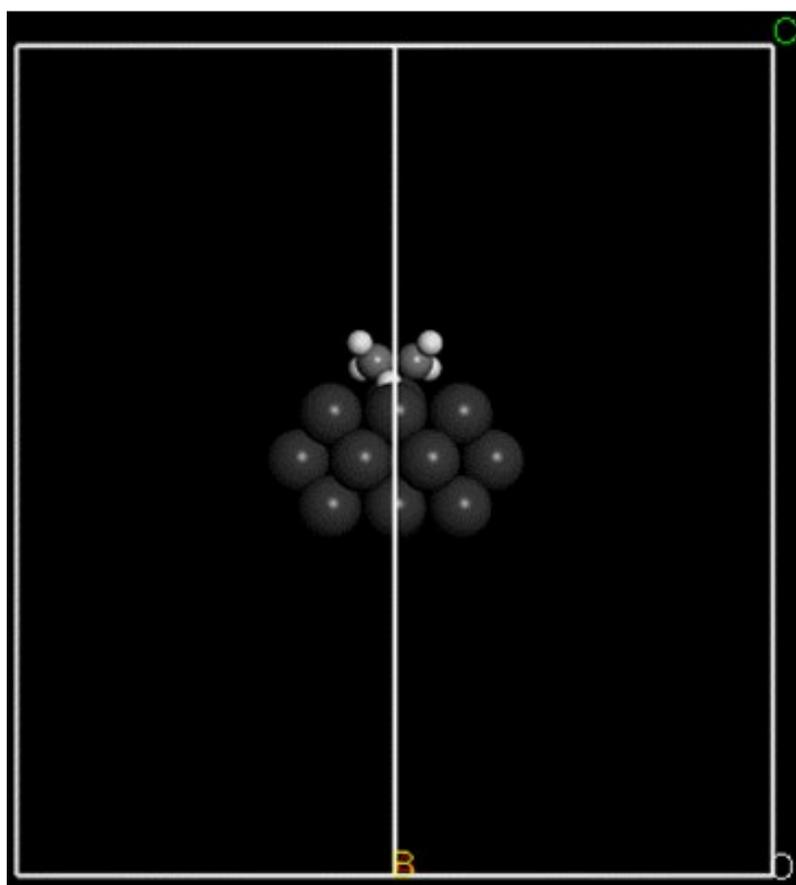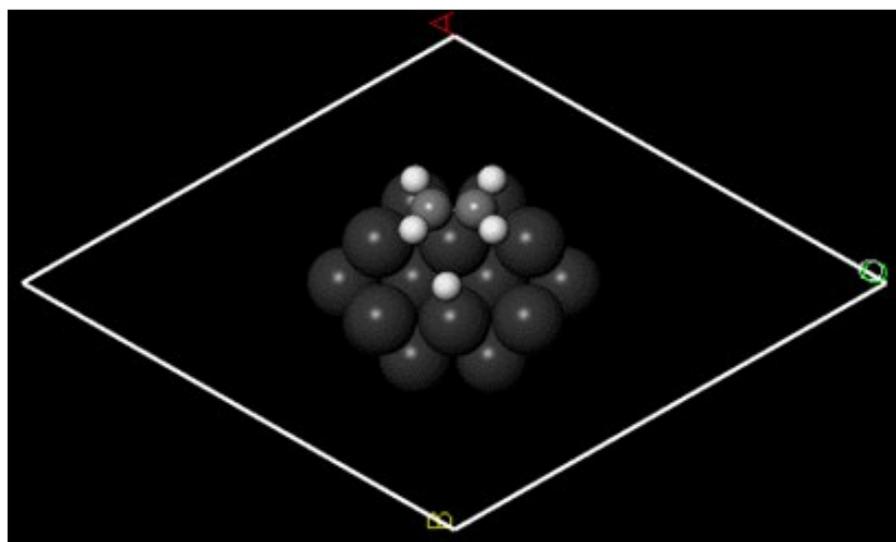
TS
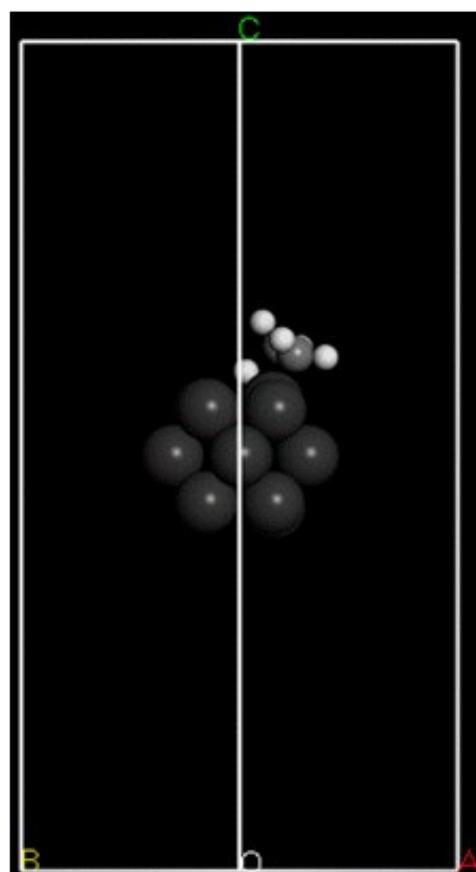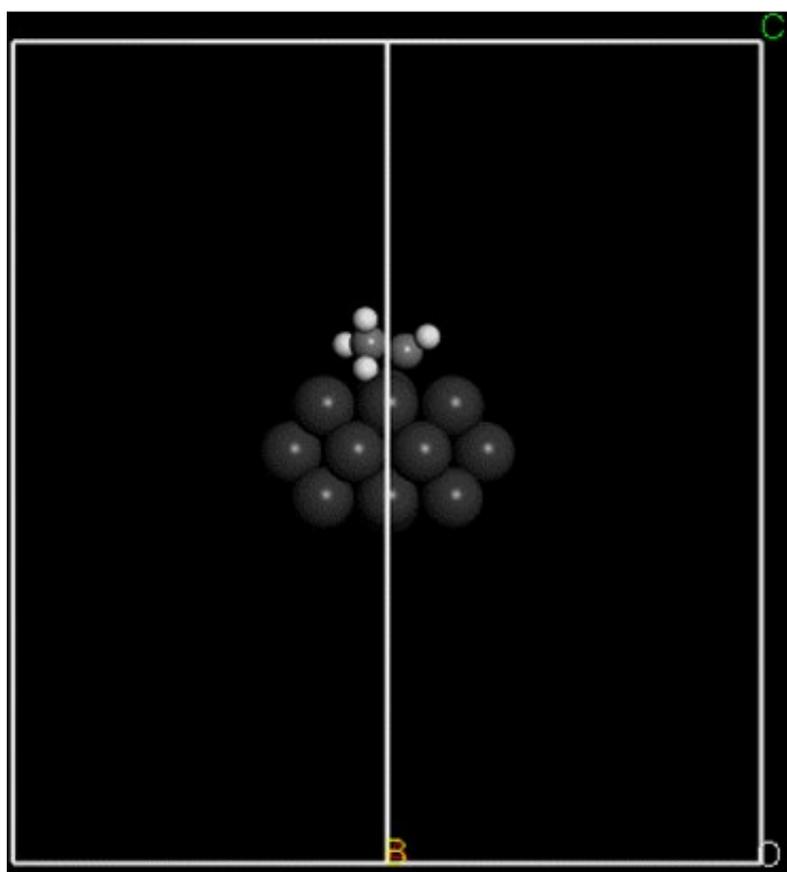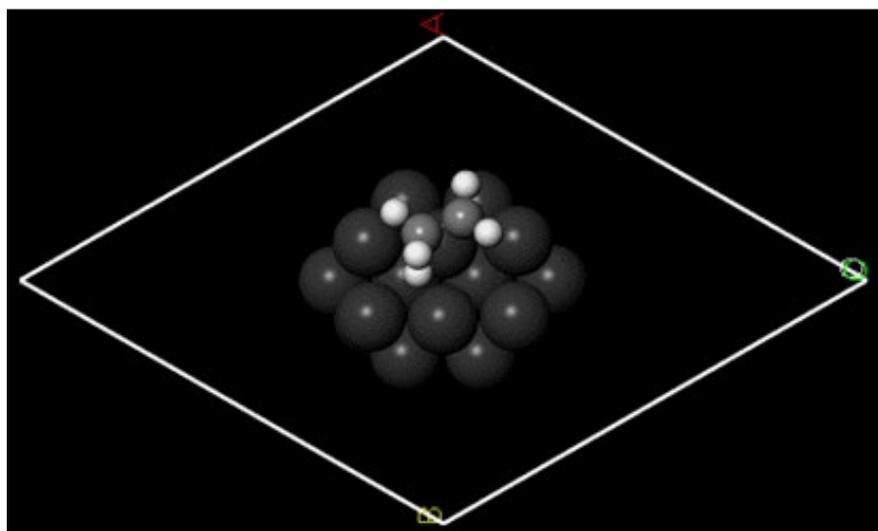
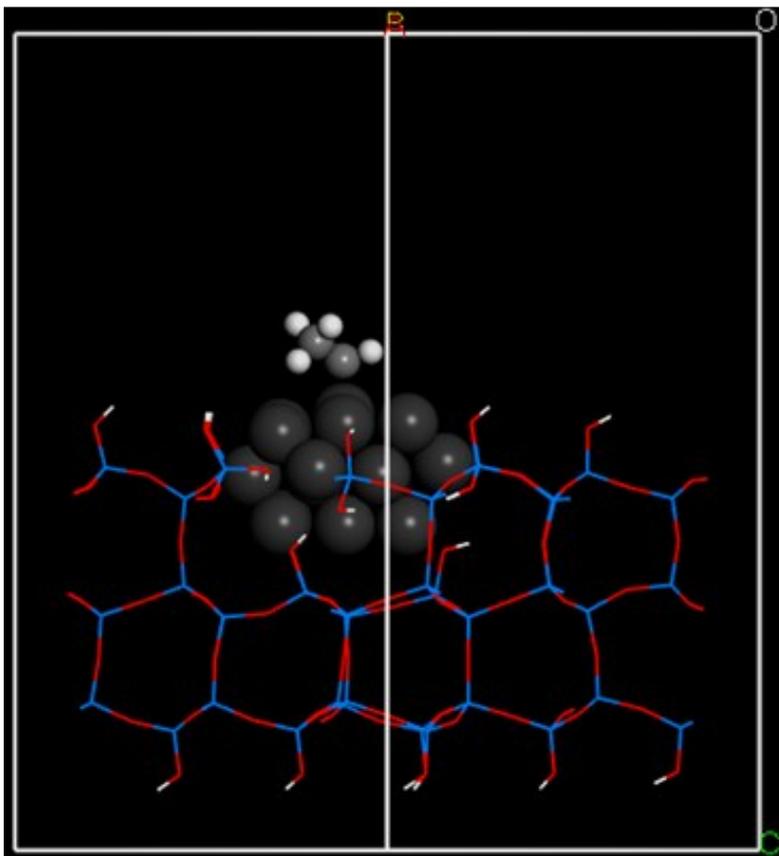FS
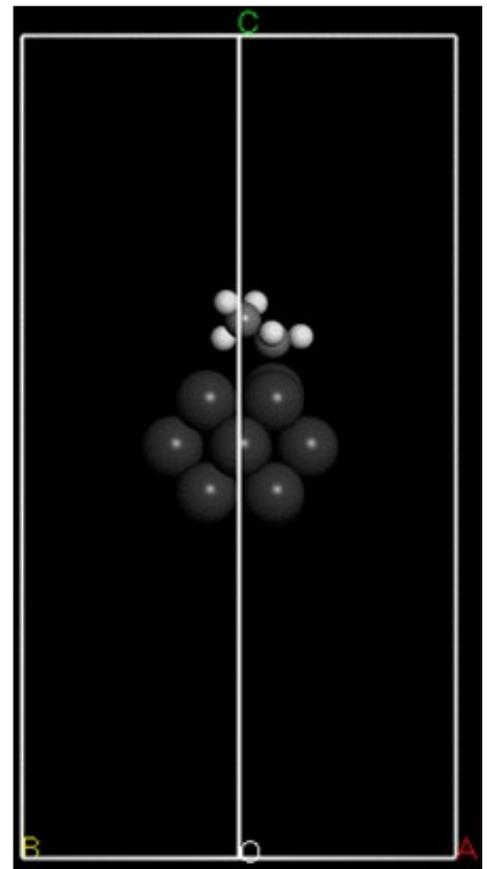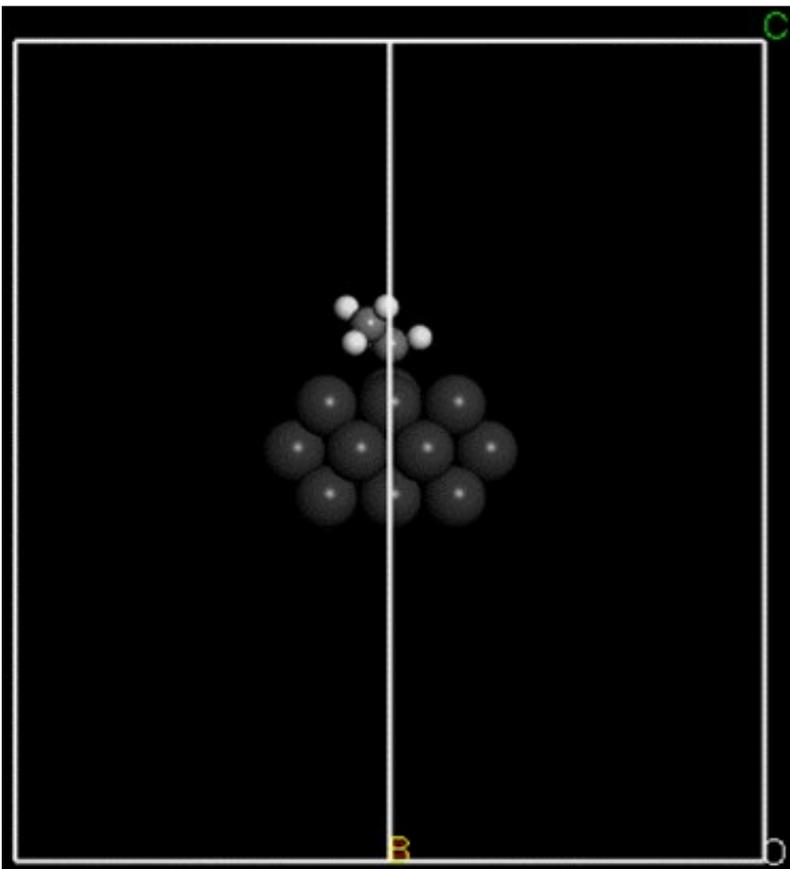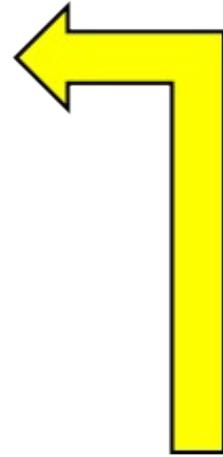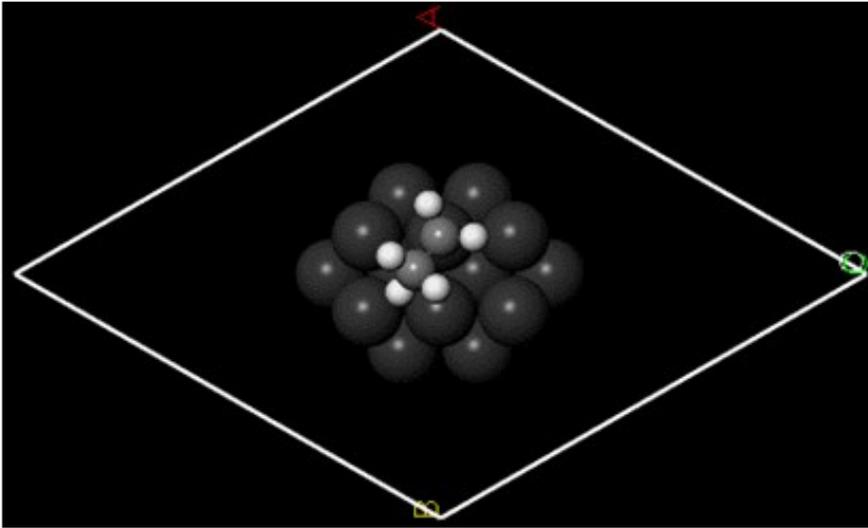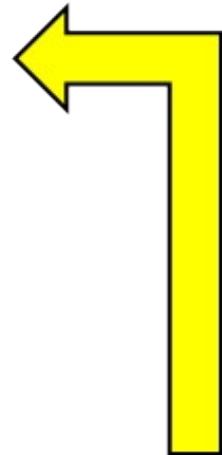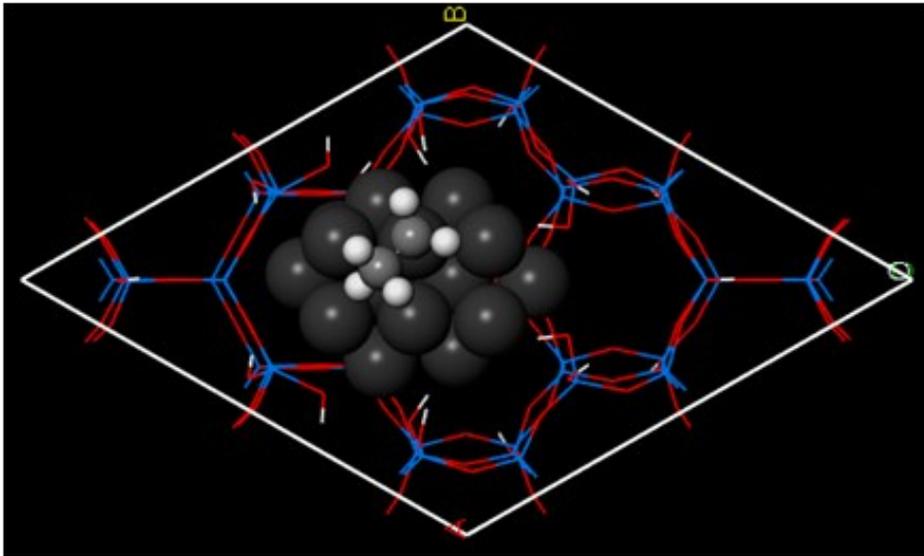
(d)   IS
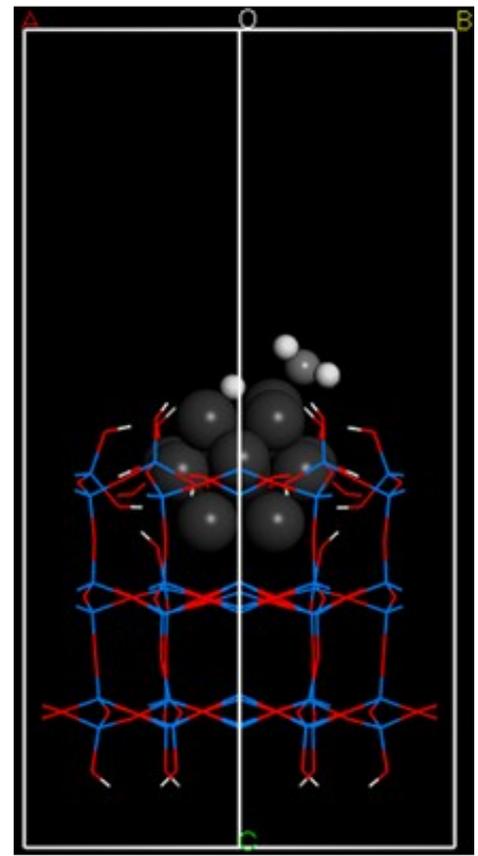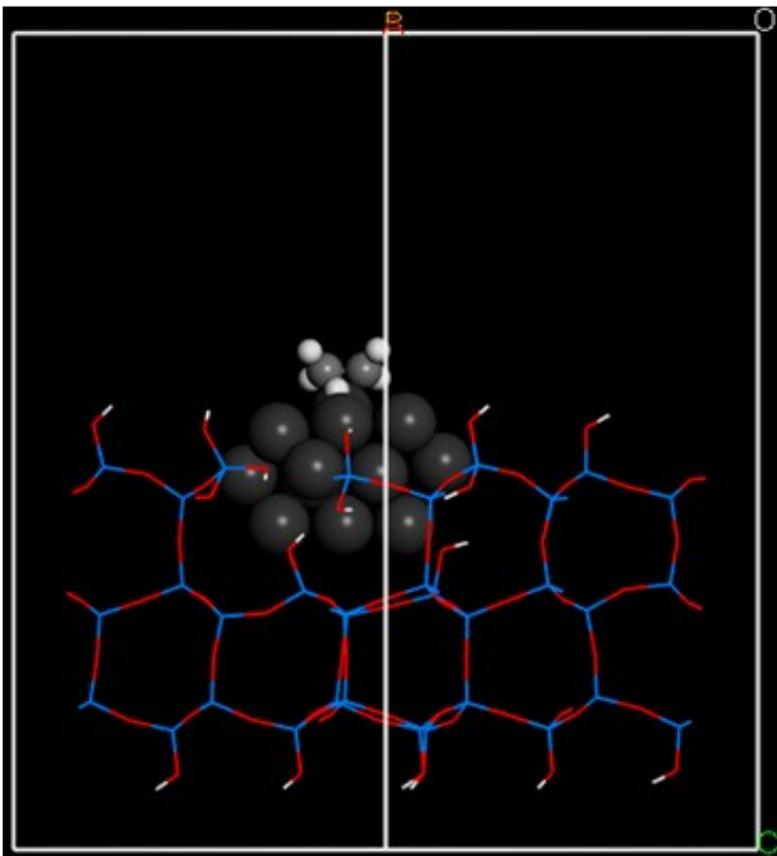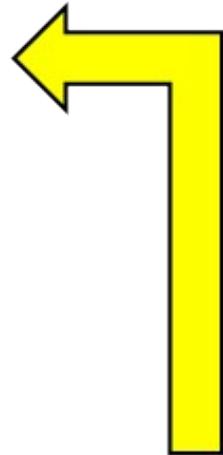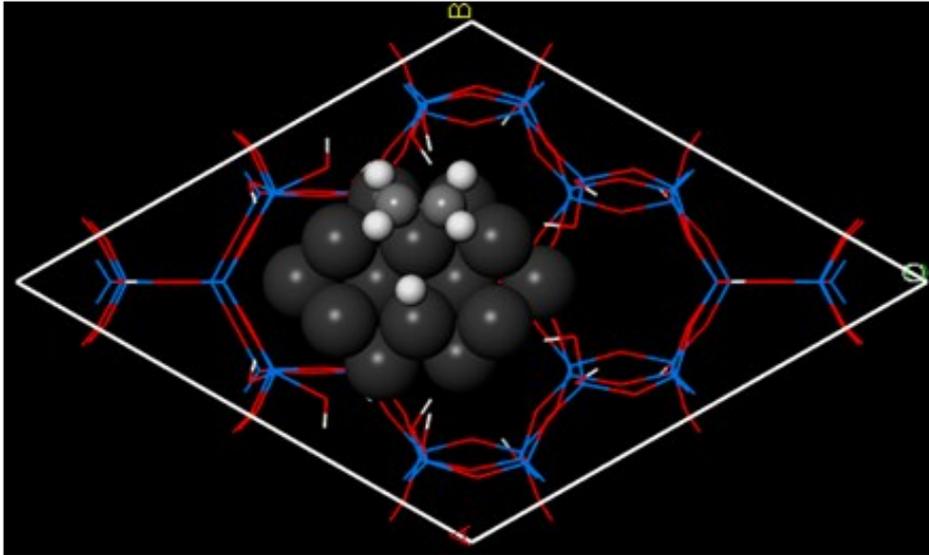
TS
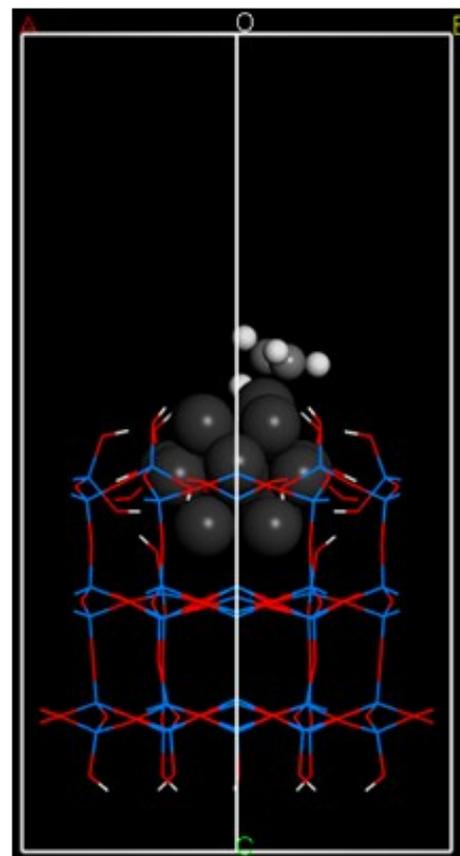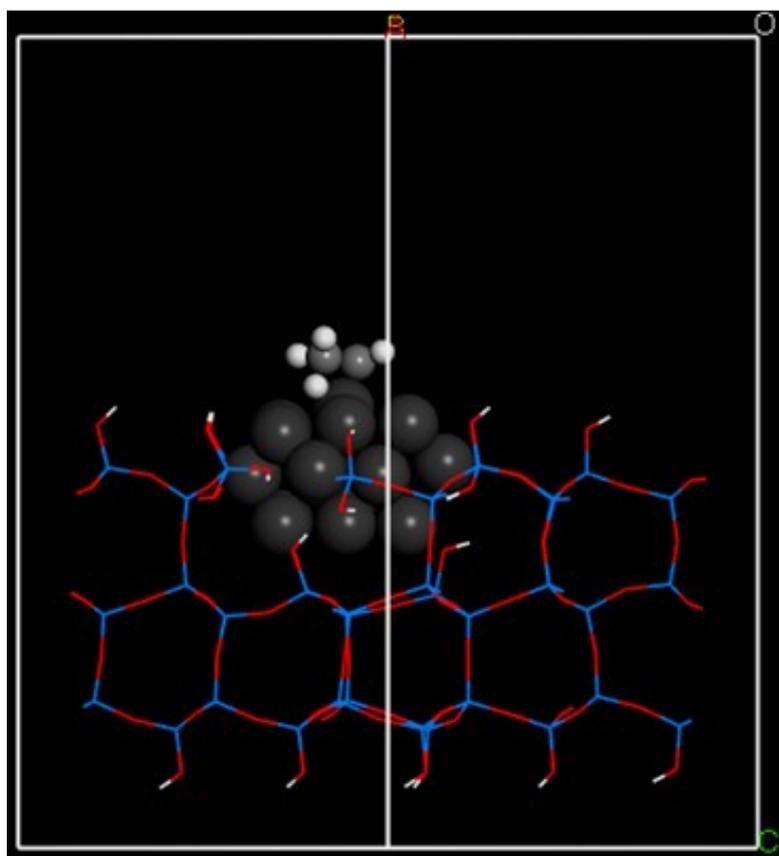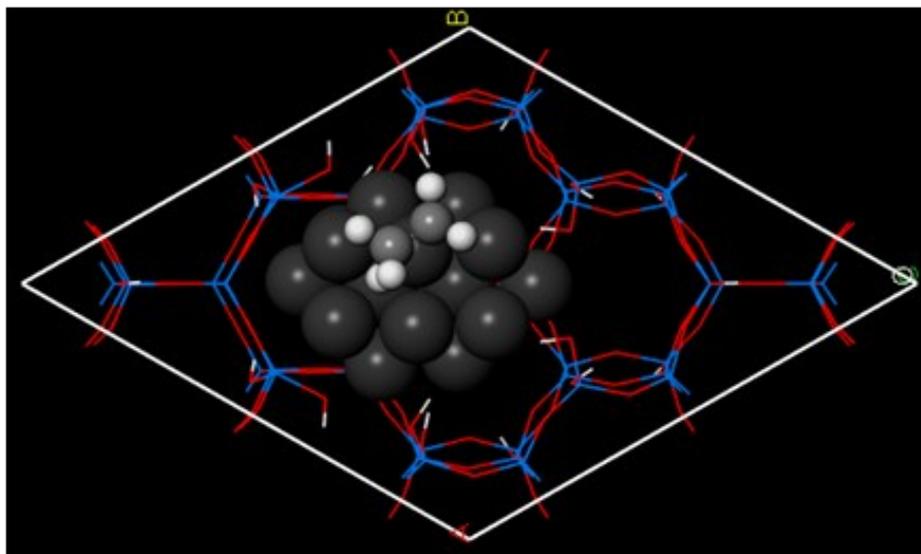
FS

Discussion on the effect of HF concentration

As shown in Figure S4, Ni dispersion and the reaction rate initially increased and then plateaued as HF concentration increased. This is probably because Ni is also dissolved by HF when the surface Ni content increases, resulting in a steady state with a certain surface Ni/Si ratio. The order of TOF at 1.0 M was $Ni_3Si \gg NiSi_2 > NiSi > Ni_2Si$, which is in accordance with that of Si content except Ni_3Si. Considersing that (1) Ni_3Si has a thick SiO_2 layer at the surface (Si-rich shell, Figure S9) and that (2) the formation of SiO_2 matrix surrounding Ni is important (Figure 5), Si-rich Ni–Si composition (at least at the surface region) would be the key factor to obtain an appropriate $Ni@SiO_2$ structure and a high catalytic performance. Ni_3Si showed a specifically high TOF at [HF] of 1.0 M and the TOF significantly dropped at the higher [HF] (Figure S4c). A possible interpretation is that the thick SiO_2 layer of Ni_3Si is completely removed and Ni-rich surface appears.

References

1.   E. Ikenaga, M. Kobata, H. Matsuda, T. Sugiyama, H. Daimon and K. Kobayashi, *J. Electron. Spectrosc. Relat. Phenom.*, 2013, **190**, 180-187.

2.   S. Tanuma, C. J. Powell and D. R. Penn, *Surf. Interface Anal.*, 1988, **11**, 577-589.

3.   M. D. Segall, P. J. D. Lindan, M. J. Probert, C. J. Pickard, P. J. Hasnip, S. J. Clark and M. C. Payne, *J. Phys. Condens. Mat.*, 2002, **14**, 2717-2744.

4.   D. Vanderbilt, *Phys. Rev. B*, 1990, **41**, 7892-7895.

5.   B. Hammer, L. B. Hansen and J. K. Nørskov, *Phys. Rev. B*, 1999, **59**, 7413-7421.

6.   A. Tkatchenko and M. Scheffler, *Phys. Rev. Lett.*, 2009, **102**, 073005-073001–073005-073004.

7.   H. J. Monkhorst and J. D. Pack, *Phys. Rev. B*, 1976, **13**, 5188-5192.

8.   N. Govind, M. Petersen, G. Fitzgerald, D. King-Smith and J. Andzelm, *Comp. Mater. Sci.*, 2003, **28**, 250-258.

9.   T. A. Halgren and W. N. Lipscomb, *Chem. Phys. Lett.*, 1977, **49**, 225-232.